ANNA GANCARCZYK, KATARZYNA SINDERA, MARCIN PIĄTEK, MARZENA IWANISZYN, MATEUSZ KORPYŚ, MIECZYSŁAW JAROSZYŃSKI, BOŻENA JANUS, TADEUSZ KLESZCZ, ANDRZEJ KOŁODZIEJ

LIQUID AXIAL MIXING IN SOLID FOAMS

Institute of Chemical Engineering, Polish Academy of Sciences, Bałtycka 5, 44-100 Gliwice, Poland

Metal and ceramic solid foams were examined to determine axial dispersion for liquids (water and 45% glycerol solution) single phase flow; the results obtained for the packed bed of spheres were used for comparison. The influence of the liquid viscosity on axial dispersion was tested. Moreover, flow resistance was also measured.

Keywords: solid foam, RTD, axial dispersion coefficient, flow resistance

Wyznaczono dyspersję osiową dla jednofazowego przepływu cieczy (wody i 45% roztworu gliceryny) przez złoże metalowych i ceramicznych pian stałych. Otrzymane wyniki zostały porównane z wartościami właściwymi dla złoża kulek. Określono wpływ lepkości cieczy na mierzony parametr. Dodatkowo wyznaczono również opory przepływu.

Słowa kluczowe: piany stałe, RTD, współczynnik dyspersji osiowej, opory przepływu

1. INTRODUCTION

Commonly used shapes of catalyst supports are: grains, spheres, pellets (used in packed-bed reactors) and monoliths. Packed-bed reactors enable satisfactory heat/mass transfer intensity, but their application leads to high flow resistance [1, 2]. These types of supports can be characterized by low porosity (0.3-0.6) [2]. On the contrary, monoliths guarantee very low flow resistance, but also poor heat/mass transfer rates [1-3]. They can be produced from ceramics (cordierite in most cases) or metals (e.g. steel).

Solid foam seems to be the modern reactor filling that combines the advantages of both catalyst supports mentioned above, i.e. packed bed and monolith. The most remarkable features of foams are high porosity (0.6-0.95) [2], high permeability, high surface to volume ratio, light weight [4]. Summarizing, foams display beneficial thermal, electrical, mechanical and acoustic properties [2, 4-6]. They can be prepared from various materials like e.g. metal (aluminium, copper) or ceramic (Al_2O_3,

cordierite) [2]. When combining the above advantages with their low pressure drop and high external surface area, it may turned out that solid foams are excellent candidates for catalyst supports [5].

At present, foams are used in aerospace industry (as wings filling), as construction material (core structures for high strength panels, mechanical energy absorbers), in heating industry (as heat exchangers), as filtering devices, heat sinks etc. [4, 5]. One possible application is also structured catalyst support in the chemical reactors. However, this field requires reliable description of the mechanisms governing the heat, mass and momentum transfer as well as of the fluid flow regimes. Knowledge of the external surface area available to active catalyst layer deposition is also crucial for proper reactor design. Axial dispersion coefficient is another key parameter for proper reactor design. Axial dispersion plays a major role in very short reactors. Modern reactors are becoming increasingly short due to continuous progress in catalysis so importance of axial dispersion is still growing in the reactors design.

While many researches can be found for gas flow through solid foams, number of studies is limited for single-phase liquid flow. Therefore, the aim of this study is the axial dispersion coefficients determination for single liquid flows through both metal and ceramic foams.

2. RESIDENCE TIME DISTRIBUTION – THEORETICAL CONSIDERATION

Each fluid element may flow through the reactor in various ways and hence at different time (Fig. 1A). The distribution of this time is called either the exit age distribution E, or more commonly the residence time distribution (RTD).

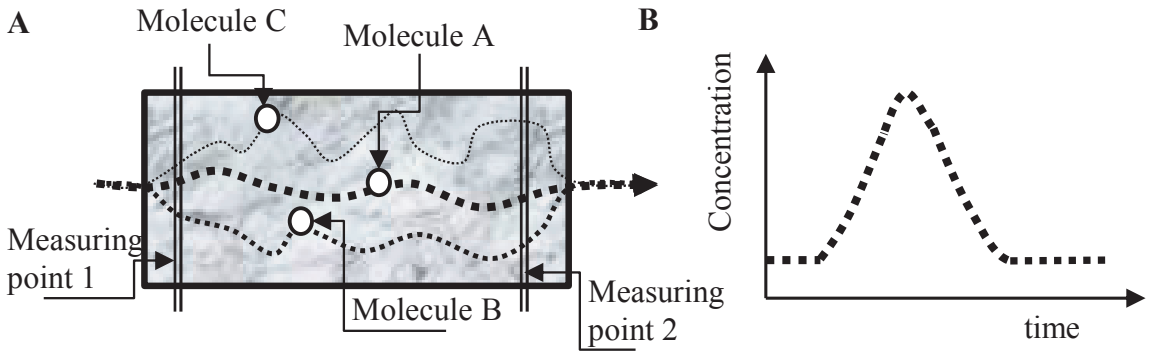

Fig. 1. Influence of the molecule's way (A) on the RTD curve (B)
Rys. 1.Wpływ drogi cząsteczki (A) na krzywą RTD (B)

The RTD curve (Fig. 1B) illustrates the fluid's molecules behaviour and it provides important information about the nature of fluid flow [7]. It is obvious that the fluid particles that chose the shorter path will appear first on the reactor outlet (Molecule A in Fig. 1A). The more tortuous is the path the longer the residence time (Molecules B

and C in Fig. 1A). Concentration of the tracer molecules (that are being injected to the fluid stream flowing via the reactor) is measured in two cross-sections: Measuring point 1 – close to reactor inlet and Measuring point 2 – near the reactor outlet (Fig. 1A) (the naming is consequently used in the article).

For a nonideal fluid flow, many different deviations from the ideal plug flow may occur, like channeling or recycling of the fluid, longitudinal mixing caused by vortices and turbulence, semi-stagnant regions, bypassing or short-circuiting [8]. Examples of these phenomena impact on the RTD curve are illustrated in Fig. 2. Appearance of stagnant zones is evidenced by curve shifting to the left side. When fluid is flowing in parallel paths double peaks can be perceived. Strong internal recirculation is suggested by many peaks with similar interspaces. There is also possibility that the tracer reacts with the reactor's content, or tracer concentration at the Measuring point 2 is measured inappropriately. In these cases the curve may be shifted to the right side [7].

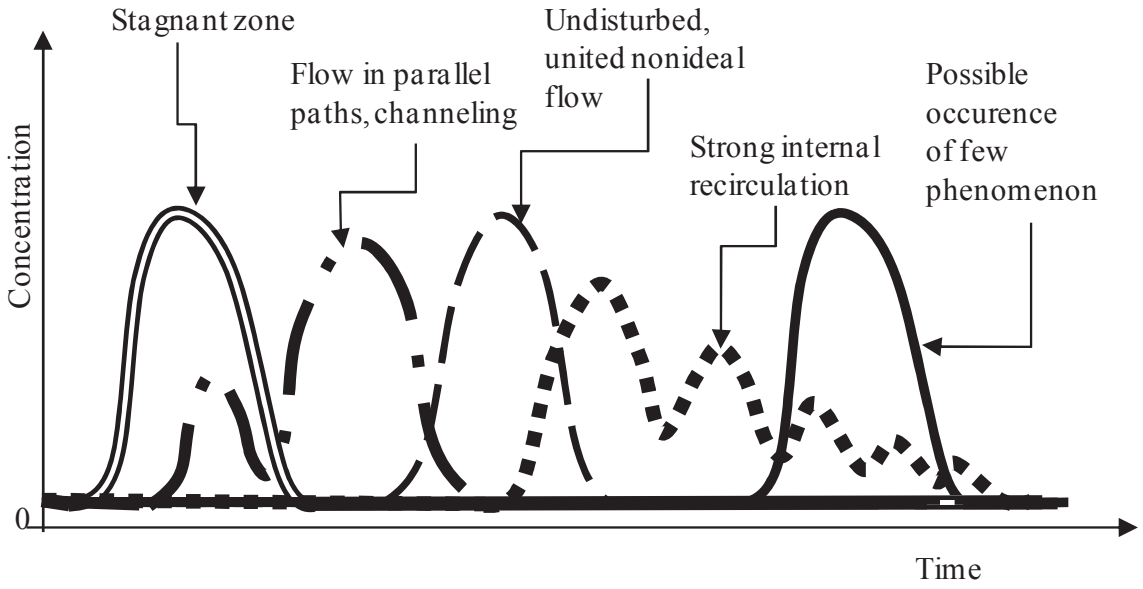

Fig. 2. Modification of RTD curve shape depending on the deviations from ideal plug flow
Rys. 2. Zmiana kształtu krzywej RTD w zależności od występujących odstępstw od idealnego przepływu tłokowego

2.1. EXPERIMENTAL DETERMINATION OF THE RTD

In order to determine the RTD curve a nonreactive tracer method is used. Tracer must not influence any component of fluid or reactor filling (in this case adsorption is also relevant). In practice only tracers with specified electrical conductivity, absorbance or emission of beta and gamma rays are used. Two possibilities of the experiment realization are easy to interpret, what makes them more popular [7]. During the first one, the tracer is injected quickly at the reactor inlet (tracer concentration vs. time inlet curve corresponds to the Dirac δ-function) – called pulse stimulus method. The Dirac δ – function assume zero values for all points except one single point, where the function value is very high. The function curve is very spiky,

narrow and precipitous [9]; the peak width equals zero but the area under the curve equals one. In the second method tracer concentration is changed instantaneously from C_0 to C_1 (step function stimulus method). Concentration of the tracer is recorded at the Measuring points 1 and 2 [8]. Both the methods mentioned above are schematically illustrated in Fig. 3.

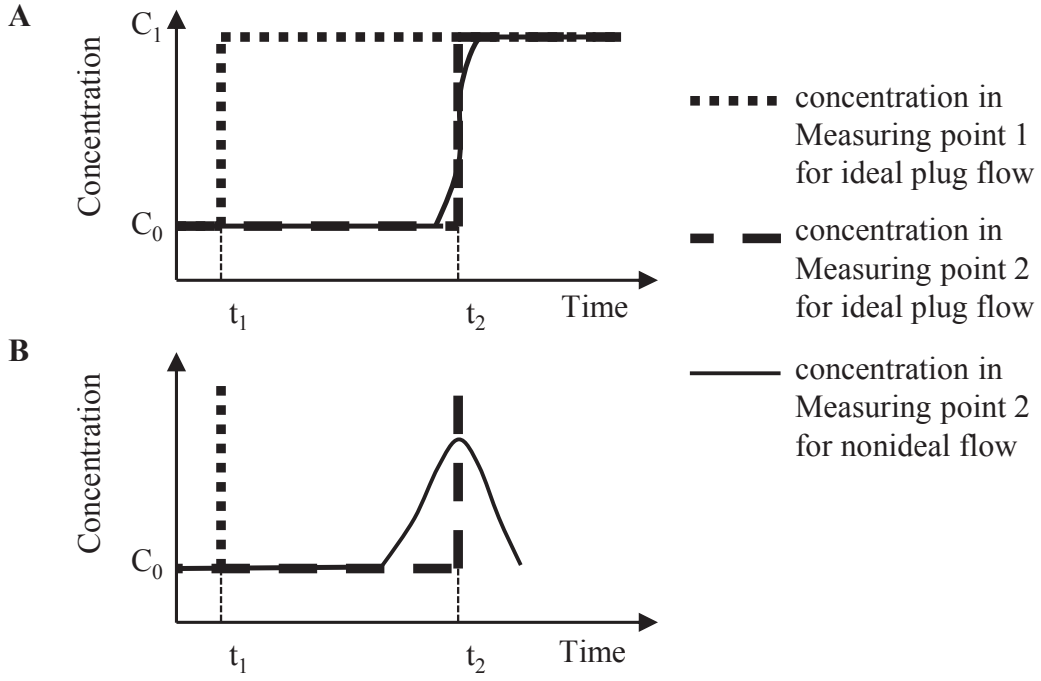

Fig. 3. RTD curves obtained by step stimulus method (A) and pulse stimulus method (B)
Rys. 3. Krzywe RTD otrzymane metodą skokowej zmiany stężenia wskaźnika (A) oraz impulsowej metody zmiany stężenia wskaźnika (B)

In reactor with ideal plug flow, tracer concentration vs. time for pulse method is identical in Measuring points 1 and 2: all the fluid molecules cross the reactor by the same way and time. For a nonideal flow, always certain deviations occur from the ideal plug flow that are immediately visible on the response curve in the Measuring point 2.

2.2. AXIAL DISPERSION COEFFICIENT: SIGLE-PHASE LIQUID FLOW

The axial dispersion coefficient, D_{ax}, can be obtained based on the mean residence time. This parameter provides information about the deviations from the ideal plug flow. The axial dispersion coefficient can be derived based on the so-called dispersion model given by the equation [7]:

$$\frac{\partial C}{\partial \theta} = \left(\frac{D_{ax}}{u_L L}\right)\frac{\partial^2 C}{\partial Z^2} - \frac{\partial C}{\partial Z} = \left(\frac{1}{Pe}\right)\frac{\partial^2 C}{\partial Z^2} - \frac{\partial C}{\partial Z} \tag{1}$$

where: Z=z/L and the Peclet number, Pe, is defined as:

$$\mathrm{Pe} = \frac{u_L L}{D_{ax}} \tag{2}$$

The larger is the Peclet number, the smaller the axial dispersion and the flow is more similar to plug one. Assuming an ideal Dirac pulse of the tracer injection, the residence time distributions is:

$$E(t) = \frac{C(t)}{\int_0^\infty C(t)dt} \tag{3}$$

2.3. TRACER RESPONSE MEASUREMENTS

There are a few ways to estimate parameters described by a dispersed plug-flow model that are presented in Table 1 [10].

Table 1. Methods of parameter estimation based on the tracer response (concentration) measurements
Tabela 1. Metody wyznaczania parametrów w oparciu o pomiar odpowiedzi (stężenia) wskaźnika

Method	Input and response function
Moment	$\int_0^\infty C_{t_1} t^n dt$, $\int_0^\infty C_{t_2} t^n dt$
Weighted moment	$\int_0^\infty C_{t_1} t^n e^{-st} dt$, $\int_0^\infty C_{t_2} t^n e^{-st} dt$
Transfer function	$F(s) = \frac{\int_0^\infty C_{t_2} e^{-st} dt}{\int_0^\infty C_{t_1} e^{-st} dt}$
Fourier	$\int_0^\infty C_{t_1} e^{-i\omega t} dt$, $\int_0^\infty C_{t_2} e^{-i\omega t} dt$
Time-domain	C_{t_1} , C_{t_2}

One of the most commonly used methods for determining parameters and describing fluid flow is the method moment. Moments m are defined as:

$$m_n = \int_0^\infty t^n C(t) dt \tag{4}$$

and the central moment is:

$$M_n^1 = \frac{m_n}{m_0} = \frac{\int_0^\infty C(t)t^n dt}{\int_0^\infty C(t)dt} \tag{5}$$

Using the moment method, the following equations can be derived:

- for the zeroth moment, which is used for checking the tracer material balance:

$$m_0 = \int_0^\infty C(t)dt = \frac{M}{V_L} \tag{6}$$

- for the first central moment, which is used to determine the mean residence time, t_m:

$$t_m = \frac{\int_0^\infty tC(t)dt}{\int_0^\infty C(t)dt} = \frac{V\varepsilon_L}{V_L} \tag{7}$$

- for the second central moment, i.e. variance, σ^2:

$$\sigma^2 = \frac{\int_0^\infty t^2 C(t)dt}{\int_0^\infty C(t)dt} - t_m^2 \tag{8}$$

Based on the formulae mentioned above, for the closed boundary conditions, the following equation connects mean residence time, variance and Peclet number can be derived [7]:

$$\frac{\sigma^2}{t_m^2} = \frac{2}{Pe} - \frac{2}{Pe^2}\left[1 - e^{-Pe}\right] \tag{9}$$

3. EXPERIMENTAL

3.1. THE FOAMS STUDIED

The open cell foams of different pore density (pores per inch – PPI) were used in this work: metallic (NC 2733 and Ni 2733, supplied by Recemat B.V.) and ceramic (Vukopor A and Vukopor S, produced by Lanik s.r.o.). The morphological parameters of the foams tested have been obtained using the computing microtomography method assisted with the iMorph software [11] and are presented in Table 2.

Table 2. Parameters of packings tested
Tabela 2. Parametry badanych wypełnień

packing	porosity, ε	geometric area, S_v, m^2m^{-3}	hydraulic diameter, d_h, mm
NC 2733	0.87	3616	0.96
Ni 2733	0.88	3411	1.03
Vukopor A 30	0.84	1386	2.42
Vukopor A 20	0.80	1113	2.88
Vukopor A 10	0.78	859	3.63
Vukopor S 20	0.71	1361	2.09
glass spheres, d_p=3 mm	0.38	1240	1.23
glass spheres, d_p=5 mm	0.388	2512	0.62

3.2.RTD EXPERIMENTS

The experiments were performed using the apparatus shown in Fig. 4.

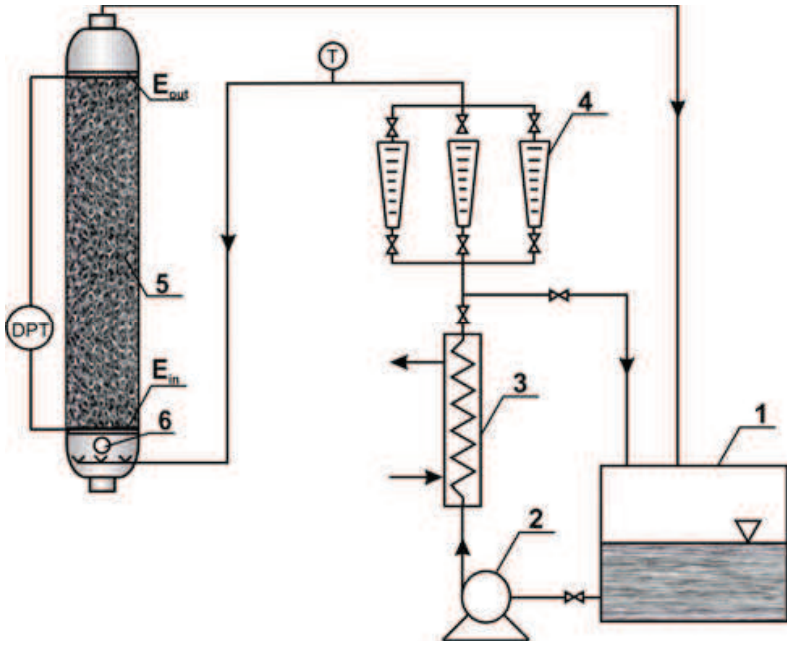

Fig. 4. Scheme of experimental set-up: 1 - liquid tank, 2 - pump, 3 - heat exchanger, 4 - flowmeters, 5 - packed column, 6 - injector, E_{out}, E_{in} - electrodes at output and inlet of the column
Rys. 4. Schemat instalacji doświadczalnej: 1 - zbiornik, 2 - pompa, 3 - wymiennik ciepła, 4 - rotametry, 5 - kolumna z wypełnieniem 6 - inżektor, E_{out}, E_{in} - elektrody na wylocie i wlocie kolumny

The column (57 mm I.D. made of transparent Plexiglas) was packed with the foam discs stacked. The high of the filling was kept within 0.5 to 0.1m. As the liquid phase, water and 45% wt glycerol solution (density ρ = 1111.18 $kg \cdot m^{-3}$ and viscosity, $\mu = 4.14 \cdot 10^{-3}$ Pa·s) were used. Liquid phase was supplied at the bottom of the column. The RTD experiments were performed using the KCl solution as the tracer (0.5 $mol \cdot dm^{-3}$) that was injected as a pulse (possibly close to the δ-Dirac function) at

the column inlet. Each injection was repeated at least three times. The signal (conductivity) was measured by two calibrated platinum electrodes placed at the column inlet and outlet. For comparison, identical experiments were performed for the bed of glass spheres (diameter of 3 and 5 mm, cf. Table 2). Additionally, the flow resistance was measured.

3. RESULTS

An example of the experimentally obtained RTD curve is presented in Fig. 5.

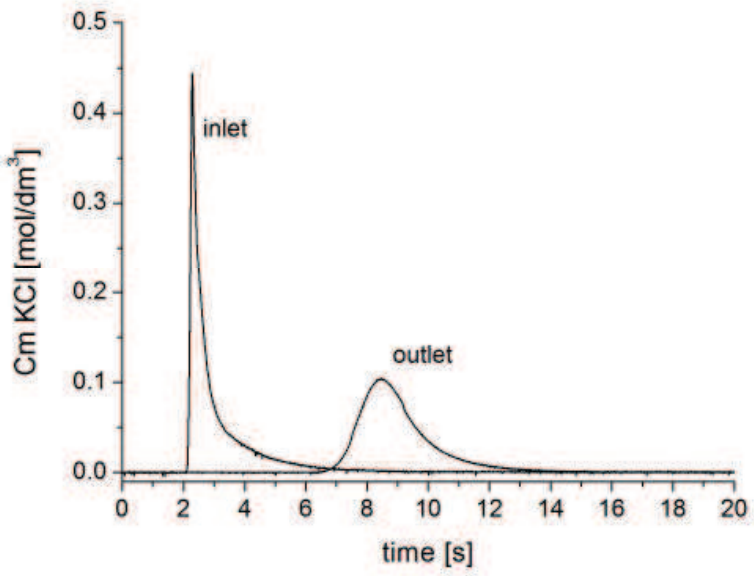

Fig. 5. An example of the experimentally obtained RTD curve
Fig. 5. Przykład eksperymentalnie otrzymanej krzywej RTD

At first, it was necessary to check whether the dead zones occur in the column. Therefore, the experimentally obtained mean residence time was compared with the theoretical one defined as:

$$t_{theoret.} = \frac{V}{V_L \varepsilon} \tag{10}$$

Good agreement between the experimental and theoretical values excluded existence of the dead zones as shown in Fig. 6 for exemplified foams. For the others, the results were similar for all the liquids applied.

The next important aspect is influence of the bed length on the axial dispersion coefficient. According to Delgado [12], the measured method is valid if the D_{ax} is constant for different bed length (assuming others experimental conditions are the same). As experimentally tested, change of the foam bed length didn't influenced the D_{ax} within 0.1 to 0.5 m (Fig. 7).

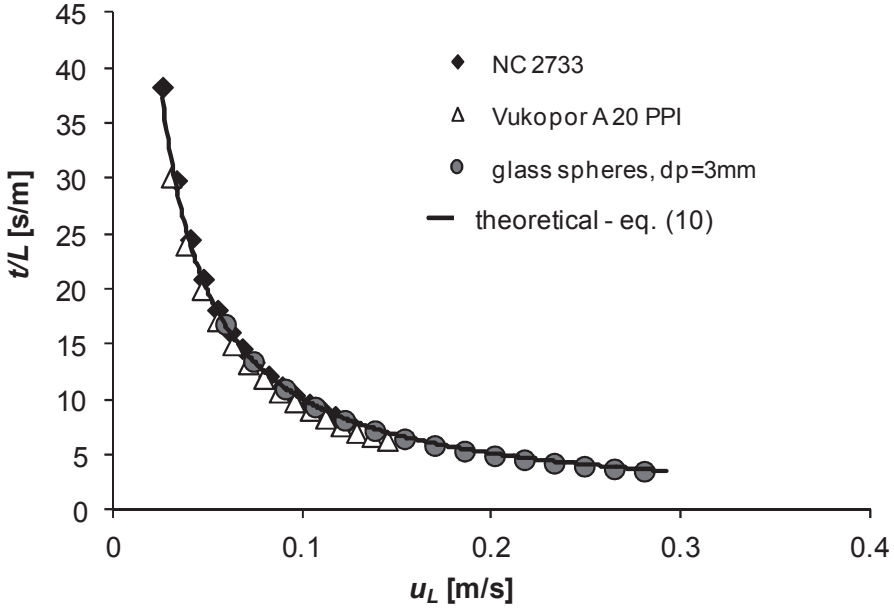

Fig. 6. Comparison of the residence time obtained experimentally and theoretically
Rys. 6. Porównanie czasów przebywania otrzymanych eksperymentalnie i teoretycznie

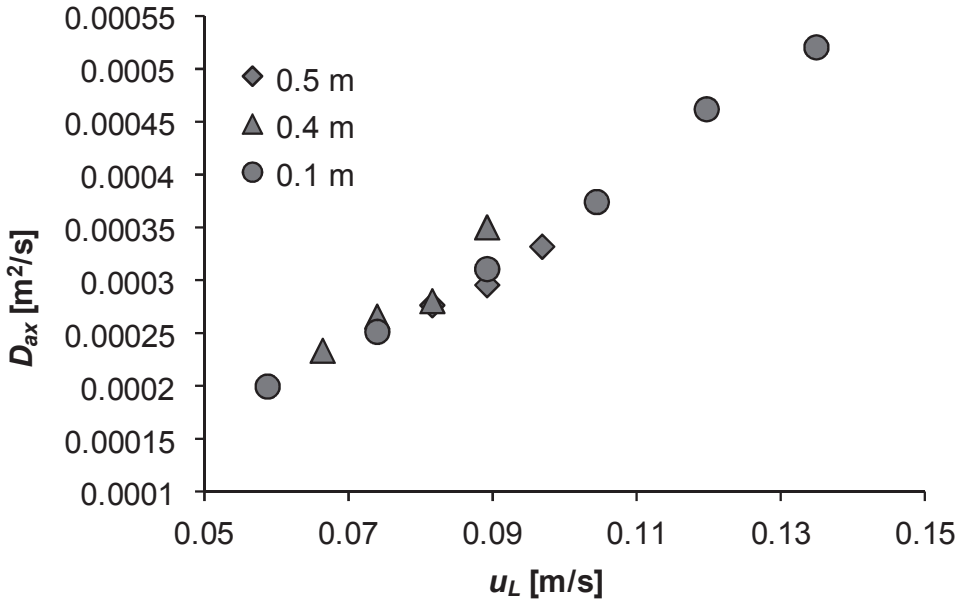

Fig. 7. Influence of the packing high on axial dispersion coefficient
Rys. 7. Wpływ wysokości złoża na współczynnik dyspersji osiowej

Fluid velocity has important influence on the axial dispersion [12]. For the superficial liquid velocity w_L range tested, the axial dispersion coefficients increase with w_L (Fig. 8) for both packing types tested (i.e. solid foams and dumped packing), as was also found for others packing types [13].

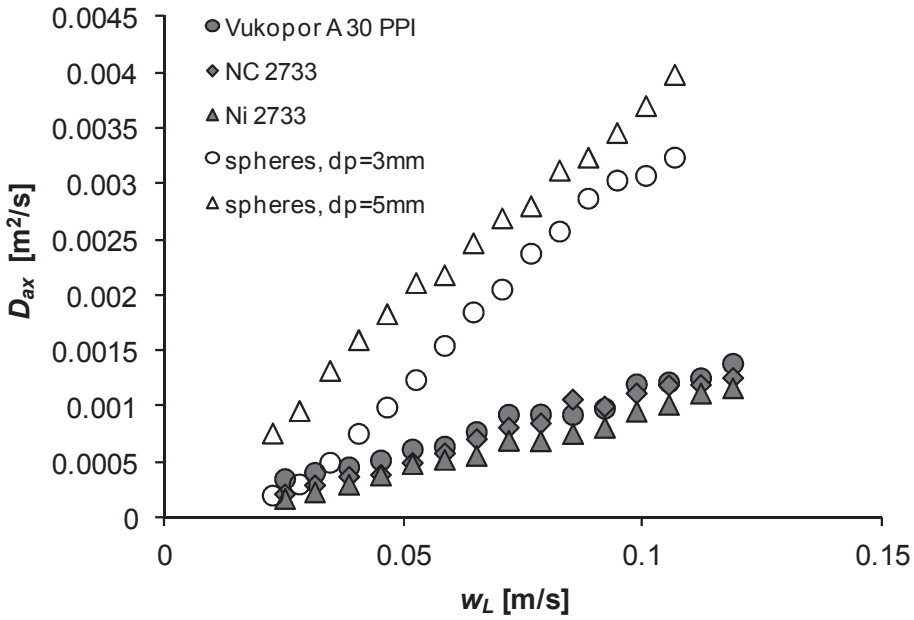

Fig. 8. Influence of the liquid velocity on axial dispersion
Rys. 8. Wpływ prędkości cieczy na dyspersję osiową

Moreover, this relationship for solid foams is almost linear and depends on pore density (PPI), i.e. D_{ax} slightly decreases with PPI number (Fig. 9) thus it increases with the pore and strut dimensions of the foams tested [6, 13]

Influence of the liquid viscosity on the axial dispersion coefficient was tested using glycerol solution. To show this influence, alternative definition of Peclet number, the so-called fluid Peclet number is used:

$$\mathrm{Pe_f} = \frac{\mathrm{u_L d}}{\mathrm{D_{axf}}} \tag{11}$$

This number uses the characteristic crosswise dimension, d, that determines the mechanical behaviour of fluids; in packed beds it is particle diameter. Usually, $\mathrm{Pe_f}$ is given versus the Reynolds number Re, because both are related to the fluid mechanical behaviour. Similar definition of Peclet number is commonly applied for solid foams, however, different values of the dimension d are used, e.g. diameter of the cell [5, 14], window [6, 15] and pore [15] as well as the hydraulic diameter [13].

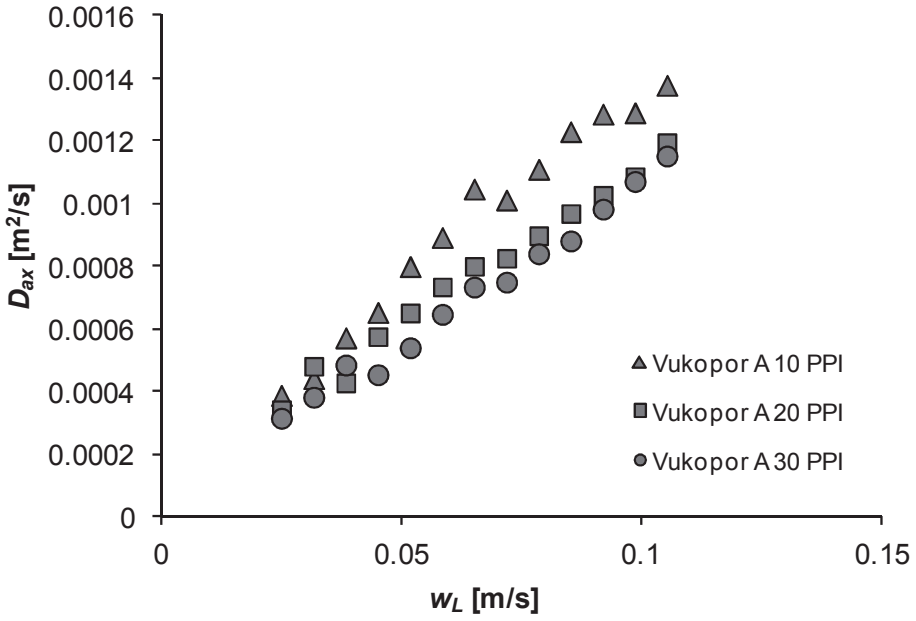

Fig. 9. Influence of the pore density (PPI number) of the solid foams on the axial dispersion
Rys. 9. Wpływ gęstości porów (liczby PPI) pian stałych na dyspersję osiową

However, when comparing different types of packings, the same definition of d should be used. Therefore, we decided to use the hydraulic diameter, d_h, as the characteristic length, defined as

$$d_h = \frac{4\varepsilon}{S_v} \tag{12}$$

The results presented in Fig. 10 prove important effect of liquid viscosity on the axial dispersion: dispersion increases with the liquid viscosity. Qualitatively, similar results were obtained for other packings [16].

Taking into account the interstitial liquid velocity, the axial dispersion coefficient can be described by a simple equation correlation in the form:

$$D_{ax} = 0.011 \cdot u_L^{1.06} \tag{13}$$

which, with the average error and standard deviation equals 13% and 8.2%, respectively, describes all the experimental points (irrespective of the foams and liquids), as shown in Fig. 11.

In addition, for the packings tested pressure drop was measured for single-phase liquid flow. It is well known that the flow resistance, $\Delta P/L$, increases with the fluid velocity [17-19] as shown in Fig. 12.

The pressure drop for solid foams is lower in comparison to the random packing; this agrees with the results for the gas flow [20].

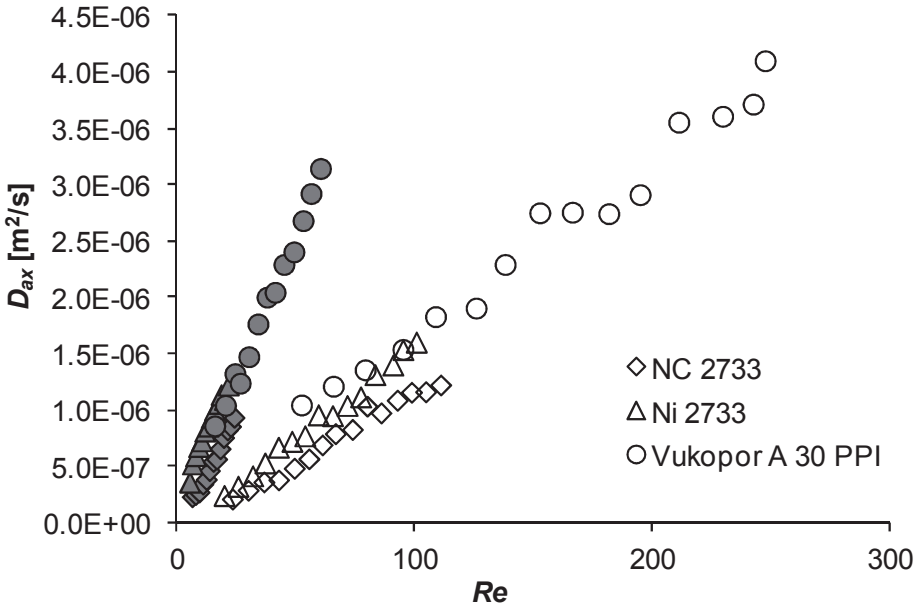

Fig. 10. Influence of the liquid viscosity on the axial dispersion coefficient; white point - water, gray point - 45% glycerol solution

Rys. 10. Wpływ lepkości cieczy na współczynnik dyspersji osiowej, białe punkty - woda, szare punkty - 45% roztwór gliceryny

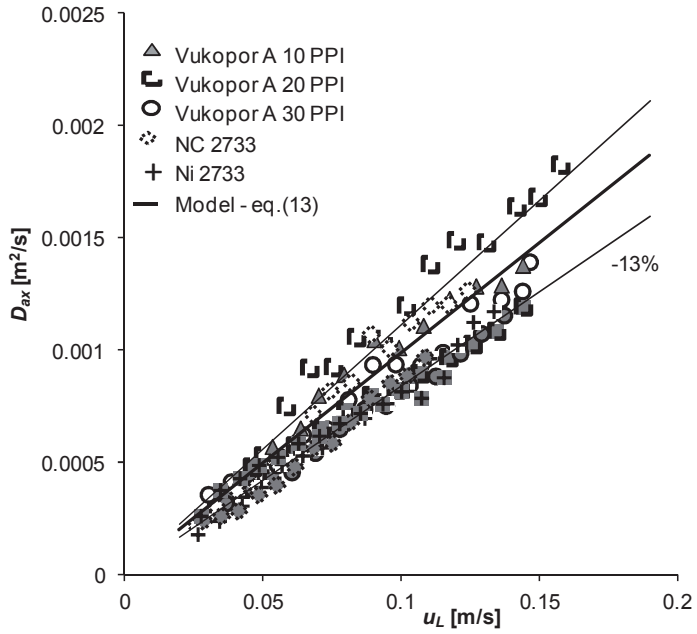

Fig. 11. Comparison experimental and calculated (eq. (13)) values of the axial dispersion. Empty symbols - water, grey symbols - 45% glycerol solutions

Rys. 11. Porównanie eksperymentalnych i obliczonych wartości dyspersji osiowej. Puste symbole - woda, szare - 45% roztwór gliceryny

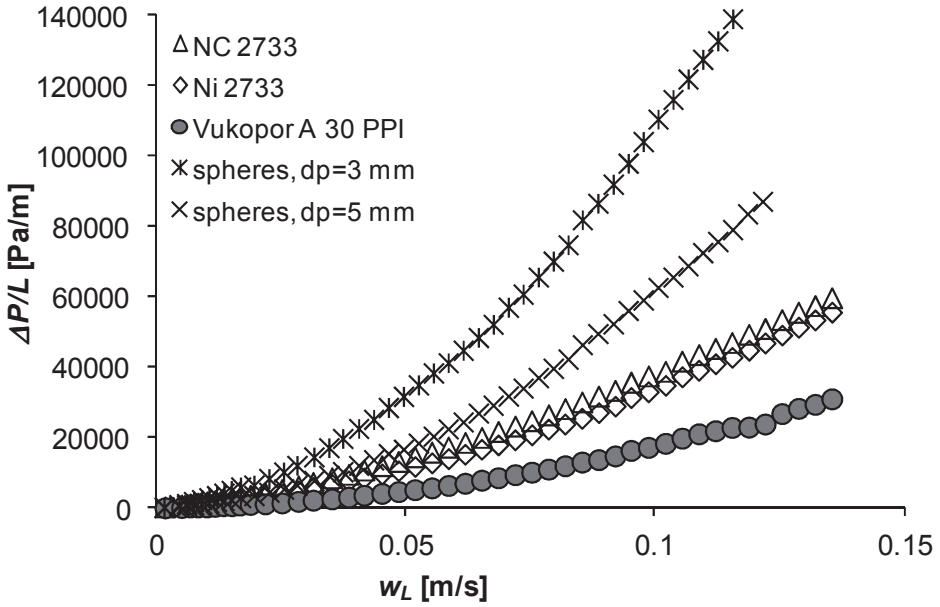

Fig. 12. Flow resistance vs. liquid velocity
Rys. 12. Opory przepływu w funkcji prędkości cieczy

For the solid foams studied, pressure drop increases with the PPI number and liquid viscosity, as shown in Fig. 13; similar observations are presented in the literature.

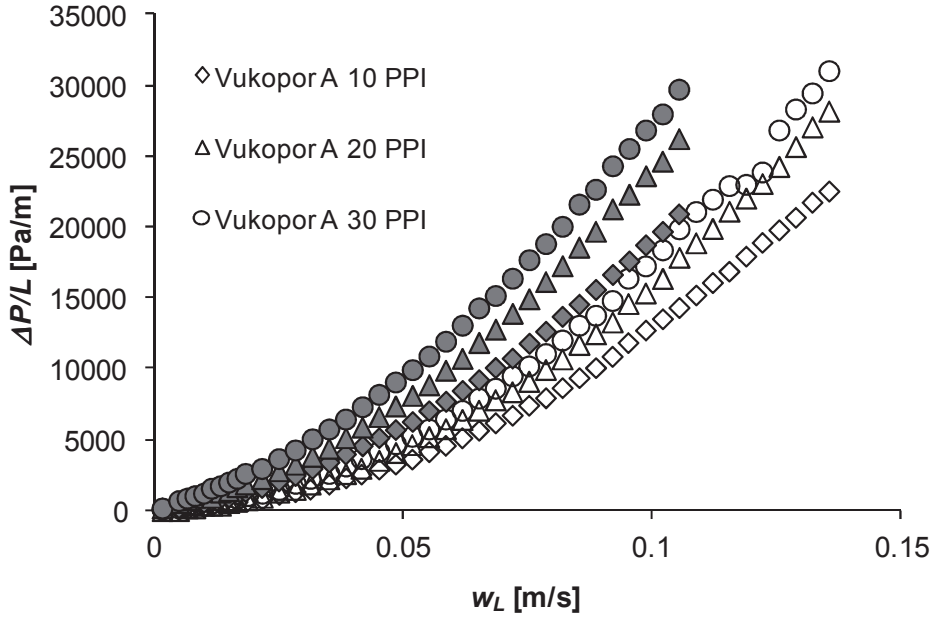

Fig. 13. Influence of the liquid viscosity on flow resistance, white signs - water, grey signs - 45% glycerol solution
Rys. 13. Wpływ lepkości na opory przepływu, białe symbole - woda, szare symbole - 45% roztworów gliceryny

CONCLUSIONS

- The axial dispersion coefficient decreases with increasing the PPI number.
- An inverse relationship was observed for the flow resistance: pressure drop increases with the PPI number, thus the flow resistance is lower for larger pores.
- The results have shown that both the flow resistance and axial dispersion increase with the fluid viscosity.
- D_{ax} for solid foams is much lower than for random packings.
- D_{ax} increases with liquid velocity.

SYMBOLS - OZNACZENIA

C	tracer concentration, mol·dm^{-3} stężenie wskaźnika, mol·dm^{-3}
C_{t1}	signal measured at Measuring point 1 (see Fig.1A) sygnał mierzony w Punkcie pomiarowym 1 (zob. Rys. 1A)
C_{t2}	signal measured at Measuring point 2 (see Fig.1A) sygnał mierzony w Punkcie pomiarowym 2 (zob. Rys. 1A)
d	diameter, m średnica, m
D_{ax}	axial dispersion coefficient, m^2·s^{-1} współczynnik dyspersji osiowej, m^2·s^{-1}
d_h	hydraulic diameter, $= 4\varepsilon/S_v$ średnica hydrauliczna, $= 4\varepsilon/S_v$
E	exit age distribution, s^{-1} rozkład czasu przebywania, s^{-1}
L	column length (height), m wysokość kolumny, m
M	mass, kg masa, kg
Pe	Peclet number, $=u_L L/D_{ax}$ liczba Pecleta, $=u_L L/D_{ax}$
Re	Reynolds number, $=u_L d_h \rho_L/\mu_L$ liczba Reynoldsa, $=u_L d_h \rho_L/\mu_L$
S_v	specific surface area, m^2·m^{-3} powierzchnia właściwa, m^2·m^{-3}
t	time, s czas, s
t_m	mean residence time, s średni czas przebywania, s
u_L	interstitial liquid velocity, m·s^{-1} rzeczywista prędkość cieczy, m·s^{-1}
w_L	superficial liquid velocity, m·s^{-1} prędkość cieczy liczona na pusty przekrój aparatu, m·s^{-1}
V	volume of the reaktor, m^3 objętość reaktora, m^3

V_L	volumetric liquid flow, $m^3 \cdot s^{-1}$ objętościowe natężenie przepływu, $m^3 \cdot s^{-1}$
z	longitudinal coordinate współrzędna wzdłużna
ε	porosity porowatość
ε_L	liquid holdup zawieszenie cieczowe
θ	dimensionless time, $=t/t_m$ bezwymiarowy czas, $=t/t_m$
σ^2	variance wariancja
ω	frequency częstotliwość

REFERENCES – PIŚMIENNICTWO CYTOWANE

[1] Piątek M, Gancarczyk A, Iwaniszyn M, Jodlowski P.J., Łojewska J., Kołodziej A., 2017. Gas-phase flow resistance of metal foams: Experiments and modeling. AlChE J., 63; 1799-1803. DOI: 10.1002/aic.15730.

[2] Edouard D., Lacroix M., Pham C., Mbodji M., Pham-Huu C., 2008. Experimental measurements and multiphase flow models in solid SiC foam beds. AlChE J., 54, 2823-2832. DOI: 10.1002/aic.11594.

[3] Huang K., Lu K., Ni S., Tong S., 2012. Studies on preparation and catalytic performances of monolithic solid acid catalysts. Asian J. Chem., 24, 997-1002.

[4] Della Torre A., Montenegro G., Tabor G.R., Wears M.L., 2014. CFD characterization of flow regimes inside open cell foam substrates. Int. J. Heat Fluid Flow., 50, 72-82. DOI: 10.1016/j.ijheatfluidflow.2014.05.005.

[5] Saber M., Huu T.T., Pham-Huu C., Edouard D., 2012. Residence time distribution, axial liquid dispersion and dynamic–static liquid mass transfer in trickle flow reactor containing β-SiC open-cell foams. Chem. Eng. J., 185-186, 294-299. DOI: 10.1016/j.cej.2012.01.045.

[6] Hutter C., Zenklusen A., Lang R., von Rohr P.R., 2011. Axial dispersion in metal foams and streamwise-periodic porous media. Chem. Eng. Sci. 66, 1132-1141. DOI: 10.1016/j.ces.2010.12.016.

[7] Levenspiel O. 1999. Chemical Reaction Engineering. Third edition, John Wiley and Sons, New York.

[8] Hill C, Root T. 2014. Introduction to Chemical Engineering Kinetics and Reactor Design. John Wiley and Sons, Hoboken, New Jersey.

[9] Kusse B.R., Westwig E.A., 1998. Mathematical Physics,.WILEY-VCH.

[10] Fahim M.A., 1982. Parameter estimation from tracer response measurement. Chem. Eng. J., 25, 1-8.

[11] Gancarczyk A., Iwaniszyn M., Piątek M., Leszczyński B., Ziółkowski G., Piech D., Janus B., Kleszcz T., Kołodziej A. 2016, Parametry morfologiczne pian stałych – metody i wyzwania. Prace Naukowe IICh PAN, 20, 63-75.

[12] Delgado J.M.P.Q., 2006. A critical review of dispersion in packed beds. Heat Mass Transfer, 42, 279-310. DOI: 10.1007/s00231-005-0019-0.

[13] Montillet A., Comiti J., Legrand J. 1993. Axial-dispersion in liquid flow-through packed reticulated metallic foams and fixed-beds of different structures. Chem. Eng. J. Bioch. Eng., 52, 63-71. DOI: 10.1016/0300-9467(93)80050-X.

[14] Saber M., Pham-Huu C., Edouard D. 2012. Axial dispersion based on the residence time distribution curves in a millireactor filled with β-SiC foam catalyst. Ind. Eng. Chem. Res., 51, 15011-15017. DOI: 10.1021/ie3017829.

[15] Mohammed I., Bauer T., Schubert M., Lange R. 2013. Hydrodynamic multiplicity in a tubular reactor with solid foam packings. Chem. Eng. J., 231, 334-344. DOI: 10.1016/j.cej.2013.07.024.

[16] Jacques G.L., Hennico A., Moon J.S., Vermeulen T. 1963. Longitudinal dispersion in single-phase liquid flow through ordered and random packings. Lawrernce Rad. Lab. Report UCRL 10696.
[17] Pangarkar K., Schildhauer T.J., van Ommen J.R., Nijenhuis J., Kapteijn F., Moulijn J.A. 2008. Structured packings for multiphase catalytic reactors. Ind. Eng. Chem. Res., 47, 3720-3751. DOI: 10.1021/ie800067r.
[18] Boomsma K., Poulikakos D. 2002. The effects of compression and pore size variations on the liquid flow characteristics in metal foams. J. Fluid Eng., 124, 263-272. DOI: 10.1115/1.1429637.
[19] Kołodziej A., Łojewska J., Jaroszyński M., Gancarczyk A., Jodłowski P. 2012. Heat transfer and flow resistance for stacked wire gauzes: Experiments and modelling. Int. J. Heat Fluid Flow, 33, 101-108. DOI: 10.1016/j.ijheatfluidflow.2011.11.006.
[20] Patcas F.C., Garrido G.I., Kraushaar-Czarnetzki B. 2007. CO oxidation over structured carriers: A comparison of ceramic foams, honeycombs and beads. Chem. Eng. Sci., 62, 3984-3990. DOI: 10.1016/j.ces.2007.04.039.

ANNA GANCARCZYK, KATARZYNA SINDERA, MARCIN PIĄTEK, MARZENA IWANISZYN, MATEUSZ KORPYŚ, MIECZYSŁAW JAROSZYŃSKI, BOŻENA JANUS, TADEUSZ KLESZCZ, ANDRZEJ KOŁODZIEJ

MIESZANIE OSIOWE W PIANACH STAŁYCH

Piany stałe posiadają wiele interesujących właściwości, takich jak np. duża porowatość, duża powierzchnia właściwa, mała gęstość w porównaniu do materiału litego, możliwość wykonywania z różnego rodzaju materiałów, co powoduje, że piany stałe rozpatrywane są jako potencjalne nośniki warstwy aktywnej katalitycznie w reaktorach wielofazowych. Jednak zastosowanie pian stałych w przemyśle wymaga znajomości wielu parametrów pozwalających na poprawne zaprojektowanie reaktora i przeniesienie skali. Jednym z nich, obok znajomości wielkości powierzchni dostępnej dla osadzenia warstwy aktywnej, oporów przepływu czy zawieszenia cieczowego, jest dyspersja osiowa, która ma obecnie szczególnie istotne znaczenie przy projektowaniu krótkich reaktorów. Obserwowany obecnie duży postęp w dziedzinie katalizy spowodował, że coraz częściej obserwowana jest miniaturyzacja reaktorów katalitycznych, w tym zmniejszenie ich długości, co przekłada się na większy wpływ dyspersji osiowej na ostateczną konwersję substratów. Dlatego celem pracy było wyznaczenie współczynników dyspersji osiowej, D_{ax}, dla złoża pian stałych oraz porównanie otrzymanych wyników z wartościami właściwymi dla złoża usypanego.

Badania wykonane zostały zarówno dla pian metalowych (NC 2733 i Ni 2733), jak i ceramicznych (Vukopor A: 10, 20 i 30 PPI, oraz Vukopor S 20 PPI). Dla porównania, eksperymenty przeprowadzono również dla złoża usypanego z kulek szklanych o średnicy 3 mm i 5 mm. Schemat instalacji doświadczalnej przedstawiono na rys. 4. Jako wskaźnik do wyznaczenia krzywej rozkładu czasu przebywania (ang. residence time distribution, RTD) zastosowano 0,5 molowy roztwór KCl.

W pierwszym etapie pracy sprawdzono poprawność prowadzonych eksperymentów; wykonane testy potwierdziły brak stref stagnacji w reaktorze (rys. 6) oraz brak wpływu wysokości złoża na współczynnik dyspersji osiowej dla złoża pian ułożonych w stos o wysokości w zakresie 0,5 – 0,1 m (rys. 7).

W oparciu o wyniki doświadczeń stwierdzono, że współczynnik dyspersji osiowej rośnie ze wzrostem prędkości cieczy, niezależnie od badanego wypełnienia (rys. 8), a jego wartość jest kilkukrotnie mniejsza dla złoża pian stałych niż dla złoża usypanego. Również lepkość płynącego płynu istotnie wpływa na wartość D_{ax} (rys. 10), co zostało sprawdzone w wyniku zastosowania wody i 45% wodnego roztworu gliceryny jako fazy ciekłej. Natomiast parametry morfologiczne pian stałych, jak np. gęstość porów (liczba porów na cal, PPI) nieznacznie wpływa na wartość dyspersji osiowej (rys. 9). Na podstawie przeprowadzonych eksperymentów opracowano równanie korelacyjne (13), które ze średnim błędem

względnym wynoszącym ok. 13% przybliża dane eksperymentalne dla wszystkich badanych pian stałych, niezależnie od stosowanej fazy ciekłej (rys. 11).

Dodatkowo wyznaczono również opory przepływu dla wszystkich badanych typów złoża oraz dla obu stosowanych cieczy. Stwierdzono, że spadki ciśnienia dla złoża pian stałych są, podobnie jak współczynniki dyspersji osiowej, znacznie mniejsze w porównaniu do złoża usypanego (rys. 12), natomiast rosną ze wzrostem lepkości cieczy (rys. 13). Jednak opory przepływu, odwrotnie niż dla D_{ax}, rosną ze wzrostem gęstości porów pian stałych.

Received: 13.11.2017
Accepted: 04.12.2017